SAHLGRENSKA ACADEMY

Investigating the Impact of Imaging Parameters on Quantification and Interpretation in Brain PET

Rim Zellaya

Master's thesis in Medical Physics

Medical Physics, 2024
Department of Medical Radiation Sciences
Institute of Clinical Sciences
UNIVERSITY OF GOTHENBURG
Supervisors: Esmaeil Mehrara, PhD; Martijn van Essen, MD PhD;
Jesus Lopez Urdaneta, MD; Susanna Jakobson, MD PhD
Examiner: Magnus Båth, Professor

MASTER'S THESIS 2024

Investigating the Impact of Imaging Parameters on Quantification and Interpretation in Brain PET

Rim Zellaya

UNIVERSITY OF
GOTHENBURG

Department of Medical Radiation Sciences
Institute of Clinical Sciences
Sahlgrenska Academy
UNIVERSITY OF GOTHENBURG
Gothenburg, Sweden 2024

Investigating the Impact of Imaging Parameters on Quantification and Interpretation in Brain PET

© Rim Zellaya, 2024

Supervisors: Esmaeil Mehrara, PhD; Martijn van Essen, MD PhD; Jesus Lopez Urdaneta, MD; Susanna Jakobson, MD PhD
Examiner: Magnus Båth, Professor

Master's Thesis 2024
Department of Medical Radiation Sciences
Sahlgrenska Academy
University of Gothenburg

Typeset in LaTeX

Abstract

Rationale CortexID software (GE Healthcare) assists in interpreting and assessing FDG and beta-amyloid brain Positron Emission Tomography (PET) images for neurological disorders. It provides Z-scores that indicate abnormal radioactive tracer uptake. These Z-scores are based on the patient's standardized uptake value ratios (SUVRs) compared to a chosen reference brain region. They reflect deviations from SUVRs in healthy individuals of the same age. A positive Z-score indicates an increased uptake and a negative Z-score indicates a decreased uptake of the radiopharmaceutical relative to the normal database. Questions have been raised whether image reconstruction parameters affect the expressed Z-scores, potentially impacting the diagnostic accuracy. This study investigates how the use of the Bayesian Penalized Likelihood (BPL) reconstruction algorithm in CortexID, with various beta-values, and the effects of Anatomical Tracers for Longitudinal Assessment and Synthesis (ATLAS) and Zero-echo-time (ZTE) attenuation correction, influence the interpretation and quantification of brain PET/MR images.

Methods List-mode PET data from 25 patients who underwent 2-deoxy-2-[^{18}F]fluoro-D-glucose (FDG) 3D static brain exams using a PET/MRI Signa 3T scanner (GE Healthcare) were reconstructed with the BPL algorithm at β-values of β50, 100, 200, 400, 600, 1000, and 1500. Attenuation correction (AC) methods, ATLAS AC and ZTE AC, remained constant as β-values varied, resulting in 14 images per patient. CortexID analyzed these images, obtaining Z-Scores. The study assessed Z-Score variations with different β-values and AC choices. *syngo*.via displayed images from one patient to visually assess parameter impact on quality and interpretation. Each image underwent analysis with two Volume-of-interests (VOIs): one on a uniform background and one on a region with high tracer uptake. Extracted max-, mean-, and peak-SUV values provided quantitative data.

Results In brain PET/MR images, higher β-values led to lower Z-Scores, and ATLAS AC showed slightly lower Z-Scores than ZTE AC. Lower β-values resulted in sharper but noisier images, while higher β-values yielded blurrier but less noisy ones. ATLAS AC produced slightly sharper images compared to ZTE AC, with an almost imperceptible difference. Max-, mean-, and peak-SUV decreased with increasing β-values in high tracer uptake regions. Mean-SUV in the uniform background remained nearly constant. Optimal image quality to the naked eye was achieved at β100-β200.

Conclusion In CortexID, higher β-values in BPL reconstruction for FDG brain PET/MR images lead to decreased Z-Scores. ZTE AC shows higher Z-Scores compared to ATLAS AC, with minimal differences in image comparison. Higher β-values lead to a reduction in max-, mean-, and peak-SUV. Additional research is needed to assess the optimal β-value in CortexID image quantification.

List of abbreviations

AC	Attenuation Correction
ATLAS	Anatomical Tracers for Longitudinal Assessment and Synthesis
BPL	Bayesian Penalized Likelihood
CT	Computed Tomography
DLB	Lewy Body Disease
FDG	2-deoxy-2-[^{18}F]fluoro-D-glucose
FTLD	Frontotemporal Lobar Degeneration
GE	General Electric
L(Y)SO	Lutetium-(yttrium) Oxyorthosilicate
LOR	Line of Response
MLEM	Maximum-Likelihood Expectation-Maximization
MRI	Magnetic Resonance Imaging
OSEM	Ordered Subsets Expectation Maximization
PDD	Parkinson's Disease Dementia
PD	Parkinson's Disease
PET	Positron Emission Tomography
PMT	Photomultiplier Tubes
ROI	Region Of Interest
SiPMs	Silicon Photomultipliers
SUV	Standardised Uptake Value
TOF	Time-of-flight
VOI	Volume Of Interest
ZTE	Zero-echo-time

Contents

1 Introduction **1**
- 1.1 Cortical regions and neurological disorders . . . 2
  - 1.1.1 The cerebral cortex . . . 2
  - 1.1.2 Common neurological disorders . . . 2
- 1.2 PET . . . 3
  - 1.2.1 Radioactive tracers . . . 3
  - 1.2.2 PET imaging . . . 3
  - 1.2.3 Attenuation Correction . . . 5
  - 1.2.4 Reconstruction algorithms . . . 6
- 1.3 CortexID . . . 7
- 1.4 Purpose . . . 9

2 Methods **10**
- 2.1 Subjects and imaging . . . 10
- 2.2 Imaging parameters and reconstruction . . . 10
- 2.3 Visual analysis . . . 11
- 2.4 Statistical analysis . . . 11

3 Results **11**
- 3.1 Statistical significance . . . 11
- 3.2 Z-Score versus β-value . . . 11
- 3.3 Visual representation . . . 13
- 3.4 Image quantification . . . 14
- 3.5 CortexID normal database . . . 16

4 Discussion **17**

5 Conclusion **21**

Appendix **25**

1. Introduction

Neurological disorders such as Alzheimer's, stroke and dementia stand as the primary contributors to both cognitive and physical disabilities, affecting approximately 15% of the global population today. Over the last three decades, the number of individuals affected by neurological disorders has significantly increased and is expected to double over the upcoming two decades [1]. It is therefore essential that the diagnostic techniques and modalities provide a detailed and reliable description of a patients condition, supporting the physicians ability to correctly diagnose the patient. One such modality, providing a detailed insight into functional and metabolic processes within a patient, is Positron Emission Tomography (PET). Unlike other imaging techniques such as Computed Tomography (CT) and Magnetic Resonance Imaging (MRI), PET imaging can provide dynamic images on molecular levels which allows diagnosis and detection of abnormalities on early stages [2].

The concept of emission tomography was first introduced in the late 1950s and has undergone continuous development by a large group of scientists up to the present day [3]. In modern nuclear medicine, PET imaging is usually combined with other modalities such as MRI and CT, enabling multimodal imaging. Clinical studies have demonstrated that the integration of anatomical structures displayed by a CT scan, or soft tissue contrast provided by an MRI, and functional information from a PET image into a single image, offers an excellent diagnostic tool and highly detailed medical images. While a PET image alone can provide functional information, it may not be adequate for a comprehensive medical assessment of a condition as there will be limited anatomical information and structural details, failing to provide the important relationship between anatomical structures and functional changes [4].

Nuclear medicine and imaging physics are closely intertwined fields. It is established that PET scans can offer a substantial amount of information regarding a patient's medical condition. However, it is critical to recognize that the quality of a PET image is highly dependent on its reconstruction algorithm and the input of the imaging parameters. A significant amount of research has been dedicated to understand how such factors affect the image quality and quantification, as they play a major role in image interpretation [5, 6]. Changes in certain image parameters can significantly alter the image quality where it can impose a great risk of hiding or improperly displaying any functional or anatomical abnormalities within a patient. In this instance, physicians may fail in correctly diagnosing the patient or leading to false negatives. Additional factors, such as patient- or machine-related artifacts, can also significantly affect the image quality and therefore it is important to ensure that these factors, mostly preventable, do not disrupt the image process or quality.

While multimodal PET scans can offer high quality medical images, allowing physicians to peer into the patients body in detail, there are additional supplementary tools today that can assist physicians in their subjective visual assessment. One such tool is the CortexID software, developed by General electric (GE) Healthcare (Marlborough, MA, USA). CortexID is relatively new to the market and is yet to be broadly utilized clinically today compared to existing medical imaging software platforms such as *syngo*.via developed by SIEMENS Healthineers. Nonetheless, CortexID has great potential to assist physicians in their interpretation process, based on its visual and regional quantitative assessment of brain PET images [5, 7]. However, prior to the clinical utilization of CortexID it is important to understand how the software interprets and processes images based on the chosen imaging parameters and reconstruction algorithms.

This study will center its attention on improving the diagnostic precision in the realm of neurological disorders when utilizing CortexID in regards to the relationship between imaging parameters and the accuracy of the results.

1.1. Cortical regions and neurological disorders

1.1.1. The cerebral cortex

The cerebral cortex which is divided into two hemispheres, is the outer layer of the human brain. In general, the cerebral cortex is responsible for the control of cognitive functions, processing information and generating voluntary movements. Because of its many folds, the cerebral cortex makes up the largest area in the brain, thereby allowing a substantial amount of information to be processed. The main cortical regions are divided into so-called lobes, including the frontal lobe, temporal lobe, occipital lobe and parietal lobe [8].

The largest lobe in the brain is the frontal lobe, located at the front of the brain just behind the forehead. The frontal lobe is responsible for problem-solving, decision-making, language, voluntary movements and personality. The motor cortex within the frontal lobe is responsible for body movements especially. The temporal lobe is located below the parietal lobe. The functions of the temporal lobe includes our memory, the ability to hear, language comprehension and the ability to convert sound to a visual image. The occipital lobe, located at the back of the head, is mainly responsible for visual interpretations, objects and facial recognition as it takes information from the retina. The functions of the parietal lobe, located above the temporal lobe, include processing sensory information such as pain, pressure, touch and position. It is also responsible for spatial processing which is the awareness of our current location and the capability of navigating ourselves around. An especially important area in the parietal lobe is the somatosensory cortex, which is specialized to represent the stimuli of touch and sensation of temperatures [8, 9].

1.1.2. Common neurological disorders

Dementia is the common name for neurological disorders that affect an individuals cognitive abilities. It can affect the memory, voluntary movements, behaviour, personality and the ability to speak. Dementia is caused by various diseases such as Alzheimer's disease, Lewy body disease, frontotemporal lobar degeneration and vascular diseases. Parkinson's disease, not falling under the definition of dementia, is also neurological disorder that affects our voluntary movements [10].

Alzheimer's disease makes up about 70% of dementia cases. The disease is long term and progressively worsens with no known treatments that can stop or reverse its progression. The disease progresses by accumulation of amyloid plaque build-up in the cerebral cortex (mainly grey matter). Amyloid plaque can have several effects on the brain cells, such as neurotoxicity by damaging brain cells, interference with neurons communication and induction of inflammation in the brain. The disease is also linked to neurofibrillary tangles, which affects neuronal structures and function, disrupted neuronal communication and cell death. Symptoms of Alzheimer's disease include memory loss, disorientation, personality changes and problems with language. Alzheimer's disease mainly affects the temporal lobe, especially in the early stages, hence the specific manifestation of the symptoms [10].

A disease that share similar characteristics of Alzheimer's disease is Lewy body disease (DLB). Similarly to Alzheimer's, the disease is progressive where abnormal proteins, so-called "Lewy bodies", accumulate in the brain. DLB can affect several cortical regions and therefore symptoms may vary depending on the stage of the disease. Characteristic symptoms of DLB include problems with cognitive functions, sleep, hallucinations, mental well-being and personality changes.

Dementia with Lewy bodies is closely related to Parkinson's disease dementia (PDD) and Parkinson's disease (PD). DLB and PDD are distinguished based on when the onset of cognitive impairment occurs. That is, PDD is characterized by the appearance of dementia, which is a progression of PD. In the earlier stages, symptoms of PD mainly affects the motor functions, such as tremors, rigidity and difficulty walking. At this earlier stage, cognitive impairment, or dementia, is usually not present and manifests itself at the advanced, later stages. Lewy bodies, leading to cell death in the brain, are present in both DLB and PDD [11].

Frontotemporal lobar degeneration (FTLD) is identified by atrophy of the brain cells in the frontal lobe and temporal lobe. It is progressed by accumulated tau proteins upon becoming abnormal or misfolded. Symptoms of FTLD include personality changes, compulsive behaviour, cognitive impairment, language problems and communication difficulties [12].

1.2. PET

1.2.1. Radioactive tracers

A radioactive tracer is a biological molecule bound to a radioactive isotope. A radioactive tracer is produced by radioactive labeling, which is substituting an atom in a biological molecule with its radioactive isotope, or by substituting a stable nuclide in a molecule with a radioactive isotope of a different element. The selection of the biological molecule depends on the specific target region within the body. In the context of brain PET, 2-deoxy-2-[^{18}F]fluoro-D-glucose, commonly referred as FDG, is the most frequently utilized radioactive tracer. FDG targets the glucose use in the brain because of the glucose component in FDG. The accumulation can indicate metabolic abnormalities in the brain if the FDG uptake deviates from normal uptake levels. Therefore, FDG is proven to be effective when searching for indications of neurological disorders [13, 14]. The isotope ^{18}F in FDG decays by positron emission, β^+ decay, with a physical half life of 109,7 minutes and a biological half life of 110 minutes. Because of the short half life, cyclotrons are usually on-site in order to spare time for the radioactive decay and completion of the PET examination.

1.2.2. PET imaging

The core principle of PET imaging is the use of radioactive tracers in order to map and visualize functional and metabolic processes in a patient. The radioactive tracer is injected intravenously which will accumulate at the target region in the patient. A PET scanner measures the emitted gamma rays from the radioisotope. The raw data from the PET scanner is then reconstructed to create an image. The image represents the distribution of the radioactive tracer in the targeted area, which can indicate the presence of abnormal changes in functional processes.

The emitted positron from ^{18}F will interact with the surrounding tissue until it collides with an electron, producing two annihilation photons. The two annihilation photons will have an identical energy of 511 keV and will be emitted in opposite directions of approximately 180°. Each photon will hit one detector in opposite directions in the detector ring and will be detected coincidentally, which means they are detected within a time-frame window of a few nanoseconds. A Line of Response (LOR) is a straight line that connects the two detectors in the detector ring where the annihilation photons were detected simultaneously. The collected LORs are used to create an image of the distribution of the tracer within a patients body. The Time-of-flight (TOF) is the time it takes for the annihilation photon pair to reach the detectors. The time measurement is extremely precise because the difference in TOF between the photons can be used to determine where the LOR occurred. TOF calculations improves the accuracy of the localization of the annihilation event, thus improving image quality.

Some acquired events originate from scattered photons or two unrelated annihilation events, see figure 1. Scatter photons, illustrated in figure 1(a) occurs when one or both annihilation photons lose some of their energy and/or direction due to interaction with the tissue before reaching the detector-ring. The loss of energy and the change in direction results in an inaccurately assigned event to the line connecting the two detectors. In the case of figure 1(b), two annihilation photons from two unrelated events result in a random coincidence, meaning they both arrive to a detector each within the coincidence time-window. The consequence of scattered photons and the two unrelated annihilation photons may contribute to background noise and image misinterpretation [15].

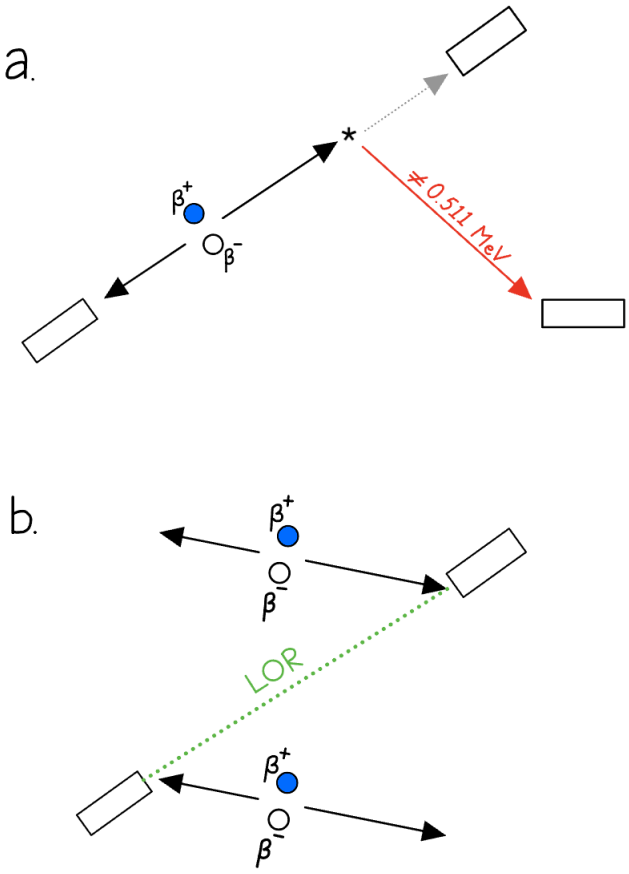

Figure 1: (a) Scatter photons and (b) annihilation photons from two different decay events. The illustration is redrawn from reference [15].

The emitted gamma rays are detected by scintillation crystals, which absorbs the annihilation photons and converts their high energy into visible light. Lutetium-(yttrium) oxyorthosilicate (L(Y)SO) is one of the most commonly utilized scintillators in a PET scanner due to its properties. LYSO scintillators have a high atomic number, high energy resolution, fast decay time and high light output, which makes them capable of handling the large amount of incoming photons. Once the gamma rays are converted into visible light, a photosensor such as photomultiplier tubes (PMT) is needed in order to convert the visible light output into an electric pulse. It is important to note that PET/MRI systems usually do not employ PMT as photosensors, instead, Silicon Photomultipliers (SiPMs) are used as photosensors. Three fundamental types of information need to be acquired from a PET detector, including where the gamma rays has hit the scintillator (position), when the output from the PMT arrives (time) and the energy of the output electronic signal. The combination of these factors enable a precise localization of the annihilation events along the LOR [16].

A sinogram is a visual representation of the collected data and provides information about the distribution of the radioactivity within the patient in the context of PET imaging. Sinograms are constructed from all the collected LORs during the data acquisition. A sinogram is a 2D matrix where the rows, or the y-axis, represents the angle of the orientation of the LOR, and the columns, or the x-axis, represents the distance displacement from center of the gantry. Therefore, each LOR corresponds to a particular pixel in the matrix. During data acquisition, a large amount of LORs are detected and the obtained sinogram will be many overlapped sine waves. An imaging reconstruction method can then be applied to the sinogram in order to obtain the final PET image [17].

During a PET scan, list-mode data is also collected. The list-mode data contains particularly useful information such as photon detection events and spatial information, which determines the detector the photon interacted with. Photon energy and arrival time to the detector are also collected. The list-mode data is continuously recorded, though the data is not processed into sinograms. List-mode data can then be utilized in image reconstruction analysis by converting the data into sinograms for certain reconstruction parameters [18]. Standardised Uptake Value (SUV) is a quantitative analysis used in PET images. It provides information about the radioactive tracer concentration in specific or selected regions in the body, thus assessing the uptake levels in those regions. SUV is normalized based on the injected dose and the patient's weight which means SUV can be a comparable variable between individuals [19].

1.2.3. Attenuation Correction

It is essential to apply an attenuation correction (AC) on the acquired sinogram before it can be reconstructed. This is because the gamma rays will attenuate differently when passing through certain densities in the body, such as bone, air and tissue. The difference in the attenuation can lead to inaccurate and inconsistent data which affects the reliability of the image. The level of attenuation depends on how long the photons travel through the body. In the context of a brain PET scan, the gamma rays travel a shorter length than through the abdomen, thus the attenuation factor is considerably larger in the abdomen than in the brain. In addition, the AC in the brain must take into account the bone, soft tissues and air-cavities, and the AC in the abdomen must also consider the air-filled lungs. The AC compensates for the absorption and attenuation of the gamma rays, which will ensure that the obtained sinogram accurately reflect the radioactive tracer distribution within the body.

Attenuation correction in PET/CT scans can be accomplished by pre-correcting the data with attenuation factors, which can be obtained from a transmission PET-scan. In CT images, Hounsfield units are used to express the pixel intensities. An attenuation map (μ-map) is a representation of the tissues attenuation properties within the body. The μ-map converts the Hounsfield units into the specific linear attenuation (μ) values for different photon energies. This conversion is accomplished using linear CT calibration curves. Another method is to incorporate the μ-map directly into the reconstruction algorithm which will attenuate correct the acquired data [20].

Unlike PET/CT AC, it is not possible to correct for attenuation using μ-maps with PET/MR systems. This is because MR images do not use linear calibration curves, since they are related to the proton densities of the tissues based on longitudinal (T1) and transverse (T2) magnetisation relaxations, rather than their attenuation properties in relation to ionizing radiation. Therefore, AC in PET/MR systems is approached differently and there are several alternative AC methods used in PET/MR [21].

Zero-echo-time (ZTE) is a sequence-based AC approach that focuses on sampling signal from tissues with very short T2*-relaxation time, resulting in T2*-weighted images. Bone is a tissue with very short T2*-relaxation time, which is particularly useful because bone has a high density in comparison to soft-tissues, thus having high attenuation properties which must be corrected. Once the T2*-weighted image is obtained from the ZTE sequence, the data undergoes tissue segmentation and classification using advanced imaging processing techniques. In this step, the different types of tissues are differentiated from the image, such as soft-tissue, air-cavities and bone. Then, linear attenuation coefficients are assigned to each tissue based on the tissue segmentation and classification, and an μ-map can be generated. The μ-map is aligned with the obtained PET data and is then incorporated in the reconstruction algorithm for a complete AC [22].

ATLAS (Anatomical Tracers for Longitudinal Assessment and Synthesis) is an additional AC method using an atlas database of previously acquired CT scans from a diverse group of individuals to create an μ-map. Since MR images are less effective at providing information about bone tissue, they are incorporated with CT images, which provide excellent bone tissue visualizations. The atlas database is used as a reference for the bone attenuation properties. The obtained patient MR images are then fused and aligned with compatible patient CT images from the atlas database. This combination generates a hybrid μ-map, where tissue segmentation and classification methods are utilized. The hybrid μ-map is then used in the image reconstruction [21, 23].

1.2.4. Reconstruction algorithms

Reconstruction algorithms are techniques used in PET imaging to convert the obtained data or sinogram into a medical image. The reconstruction of images enable a quantitative analysis by quantifying and visualizing the radioactive tracer uptake within the body, such as SUVs. Depending on the chosen reconstruction algorithm, the level of noise in images and image artifacts can be reduced, resulting in better image quality. Reconstruction algorithms can also improve the image resolution, which becomes fundamental when assessing and analyzing small lesions.

The most widely employed reconstruction algorithm is the Ordered Subsets Expectation Maximization (OSEM) algorithm. OSEM is an iterative algorithm that represents a developed and accelerated version

of the Maximum-Likelihood Expectation-Maximization (MLEM) algorithm. MLEM repeatedly iterates and reconstructs the data until it converges to the image that is the most likely given the data. OSEM operates with the same underlying principles as MLEM, though it divides the data into several subsets during the iterations. The user has the flexibility of manually adjusting the number of iterations and subsets. When the data is partitioned into subsets, the convergence will accelerate, which will significantly reduce the reconstruction time. However, an increased amount of subsets may heighten the noise levels in the image due to the low amount of statistical information in each subset. As the number of iterations increases, noise levels and decreased image quality will also be more prominent. To counteract the increased noise, the number of iterations are usually limited to 2-4 iterations, though at the expense of potentially distorting smaller lesions, and the quantitative accuracy may also be compromised. The OSEM reconstruction algorithm is described by equation 1,

$$\hat{x} = \arg\max_{x \geq 0} \sum_{i=1}^{n_d} y_i \log[Px]_i - [Px]_i, \tag{1}$$

where y_i is the acquired data, x is the estimated image and P is the physical system geometry matrix that describes how the data is acquired [24].

Bayesian Penalized Likelihood (BPL), also known as Q.Clear, is a reconstruction algorithm recently developed by GE Healthcare. It operates under the same conditions and principles as OSEM reconstruction algorithm, though the difference is the introduction of an additional term, namely the "penalized likelihood" term. The BPL reconstruction algorithm is described by equation 2,

$$\hat{x} = \arg\max_{x \geq 0} \sum_{i=1}^{n_d} y_i \log[Px]_i - [Px]_i - \beta R(x) \tag{2}$$

where $R(x)$ is the penalty term and β controls the strength of the penalty term. The penalty term controls the noise and eventual artifacts in the reconstructed image. It is particularly useful in reducing noise levels compared to OSEM and improving the image quality. The β value is adjusted by the user, allowing a balance between image noise reduction and image details. A lower beta value produces an image with fine details but with less noise reduction, and a higher beta value reduces the noise but compromises on the detail resolution.The β value can be adjusted to achieve a balance between reducing noise in the background and preserving details in the image. The partitioning of data into subsets in OSEM is not mandatory in BPL. Instead, BPL utilizes a block-sequential approach where the image and the data are divided into blocks, allowing every voxel in the image to converge. With each iteration, the blocks of data are updated instead of updating the entirety of the image data at once. This may allow an improved reconstruction efficiency while maintaining image quality [24].

1.3. CortexID

CortexID is a software utilized for quantification and analysis in FDG and beta-amyloid brain PET images. The software includes SUV ratio (SUVR) normal database from a wide range of age-matched healthy controls. The normal database from the healthy controls is based on PET/CT examinations with OSEM reconstruction, where varying matrix sizes and FOV's, along with multiple vendors, were in-

cluded. The main purpose of CortexID is to evaluate pathological changes by quantifying the patient's radioactive tracer uptake levels relative to certain reference areas within the brain. CortexID accomplishes this by quantifying the radioactive tracer uptake levels in the cortical regions from the patient, resulting in SUV's. Then, CortexID divides the SUV from each individual cortical region by the SUV in a selected reference region. This division of SUV's result in SUVR's i.e a ratio. The SUVR from each cortical region from the patient is then compared to the SUVR's from what a healthy control would have with the same reference region. The healthy levels of SUVR's for each cortical region are in the CortexID normal database, and they are also age-matched.

In order to determine if there are any pathological changes in the brain based on the SUVR's from the patient and the normal database, CortexID expresses its results as so-called Z-scores. These Z-scores determine how many standard deviations there are from the patient's SUVR's to the normal databases SUVR's. The Z-scores are therefore expressed for each cortical region in the brain, where Z $\geq$ 2.0 or Z $\leq$ -2 is considered significant. The Z-scores are calculated according to equation 3,

$$Z = \frac{x - \mu_{\text{normal}}}{\sigma_{\text{normal}}} \tag{3}$$

where x is the patient's SUVR, denoting the patient's radioactive tracer uptake levels relative to a reference region, μ is the normal SUVR, denoting the normal radioactive tracer uptake levels from the healthy controls relative to the same reference region, and σ is the standard deviations from the μ. A positive Z-score indicates an increased uptake and a negative Z-score indicates a decreased uptake of the radiopharmaceutical relative to the reference data. If the Z-score is equal to, higher than 2 or lower than -2, it is considered that there may be an abnormality within that region.

Displayed images from CortexID in Figure 2 exemplifies how abnormal radioactive tracer uptake appears visually compared to uptake distribution levels from the normal database. The left image in Figure 2 is a Z-score map, that maps the difference between the patient's radioactive uptake and the normal mean. In the Z-score map, black and blue illustrates little or no difference between the patient's uptake levels and the normal database, whereas orange and red represent large differences. The image in the middle in Figure 2 is the obtained registered patient PET/MR image, highlighting areas in the brain with an increased or decreased radioactive tracer uptake. The right image is the age-matched normal mean cortical uptake from the CortexID normal database. Figure 3 illustrates how the CortexID Z-score values are expressed in the software.

CortexID is a particularly beneficial supplementary tool that assists in the clinical interpretation of brain PET images. In addition, the software presents the distribution of FDG uptake throughout the entire brain, encompassing subcortical structures. This information is visually represented through axial, coronal, and sagittal images for analysis. Additionally, the software provides 3D stereotactic surface projection (3D-SSP) maps, illustrating uptake ratios, along with voxel-based Z-score distribution maps covering the brain cortex and cerebellum. The user also has the flexibility of analyzing and displaying a PET-only image, MR-only image or a merged PET/MR image [5, 7].

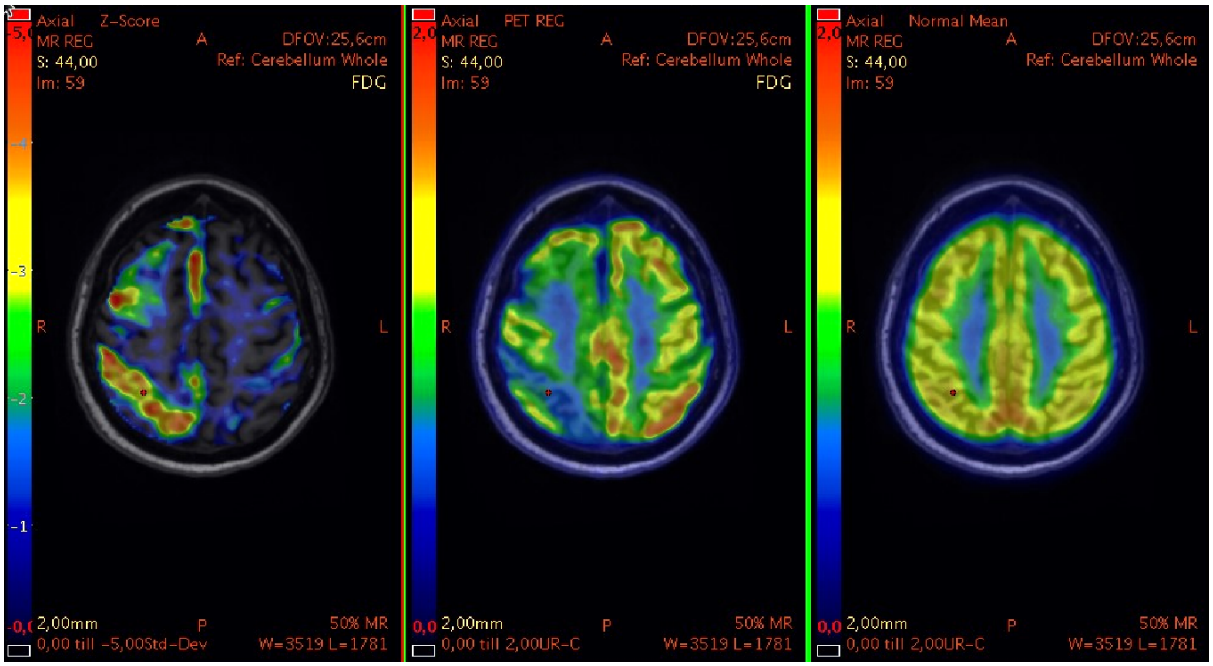

Figure 2: Displayed PET/MR images in CortexID. The left image is a Z-score map, the image in the middle is the obtained patient PET/MR image, and the right image is the normal mean radioactive tracer uptake distribution for a healthy control.

Figure 3: Expressed CortexID results in the application.

1.4. Purpose

The study investigated the effects of the BPL algorithm on PET/MR image reconstruction within CortexID, considering that CortexID utilized a normal PET/CT image database without BPL reconstruction, and therefore no β-values were included. As PET imaging system characteristics and reconstruction parameters profoundly impact image quality and quantification accuracy, our investigation explored how employing BPL reconstruction with varying β-values and attenuation correction in a PET/MRI system

affected the image interpretation and quantification of FDG uptake in cortical regions. The goal was to evaluate the extent of those effects considering the potential diagnostic implications due to variations in image quantification. Additionally, the study aimed to identify a BPL reconstruction that produced reliable results when analyzed with CortexID.

2. Methods

2.1. Subjects and imaging

List-mode PET data was accessed from patients between the age 30 and 85 years who underwent 3D static brain PET/MR examinations at Sahlgrenska University Hospital. The primary focus was choosing data from patients that were examined for neurological disorders using FDG tracer. The data acquisition was performed by a PET/MRI Signa 3T (GE Healthcare, Marlborough, MA, USA) scanner. A total of 25 patient's list-mode data from February 2023 to October 2023 was included in the study, where four of them were healthy patients. Patient diagnosis and information were accessed through their charts and by their physicians medical assessment. All patient information and data was anonymized in the PET/MR console.

2.2. Imaging parameters and reconstruction

The PET list-mode data underwent reconstruction using the BPL (Q.Clear) reconstruction algorithm. The two varied imaging parameters were the β value and the choice of attenuation correction. The choice of the utilized β values in this study were determined upon prior research findings. The included β values encompassed β 50, 100, 200, 400, 600, 1000 and 1500. The selection of the attenuation correction methods included ATLAS AC and ZTE AC. Specifically, when the β value was varied, the AC remained constant. However, neither of ATLAS AC and ZTE AC is considered to be the ideal or reference AC, as only their effect on the Z-scores were analyzed in this study and how the two AC compare generally, while also considering that it is unknown which AC was employed in the CortexID normal database. The same rationale is applied to the choice of β values, considering that the CortexID normal database did not use any β values Consequently, each patient yielded 14 reconstructed images, where seven images featured ATLAS AC and the other seven utilized ZTE AC. All reconstructed images incorporated corrections for deadtime and scatter, with the inclusion of TOF and point-spread function (PSF). The field-of-view (FOV) for the images measured 25 cm with a 256 x 256 matrix.

The reconstructed images were stored in the GE Advanced Workstation (AW) server 3.2 where the images were accessed through CortexID Suite 2.1 Ext. 6. The choice of the MR image was AX T2 PROPELLER and the reference region was set to Cerebellum Whole with FDG tracer for all reconstructed images. Subsequently, the images underwent analysis using CortexID and the results were displayed as Z-scores as exemplified in figure 3. The Z-score results were saved as tables in CSV-files which were later used in the statistical analysis.

2.3. Visual analysis

Moreover, reconstructed images from one of the patients, randomly selected, were also accessed and displayed through *syngo*.via. This was done in order to visually assess the impact of varying image parameters on image appearance and interpretation employing the widely adopted imaging software platform *syngo*.via. A total of seven images with the varying β values, each employing ATLAS AC, and another seven with ZTE AC were displayed. One radiologist visually assessed the overall appearance of the 14 images sharpness and blurriness, but no proper analysis of image noise and contrast levels was conducted in this study. A volume-of-interest (VOI) was applied on all 14 displayed images on the same region where the max-, mean- and peak-SUV values were extracted. Finally, a graph was generated illustrating the relationship between the maximum SUV and the varying β value.

2.4. Statistical analysis

Python and Excel were used for the statistical analysis. Repeated Measures ANOVA (RMA) was employed on the acquired data to test for statistically significant differences between the obtained Z-scores when varying the β values and using ATLAS and ZTE attenuation corrections. A confidence interval of 95% with a significance level of 0.05 was used.

3. Results

3.1. Statistical significance

The RMA analysis demonstrated statistical significance ($P < 0.05$) for all cortical regions analyzed by CortexID, except for Parietal Superior R ($P > 0.05$), when comparing the means of the Z-Scores with respect to the varying β-value. The paired t-test comparing the means of Z-Score results when using ATLAS AC and ZTE AC also showed statistical significance ($P < 0.05$) for all cortical regions, except for Temporal Mesial R, Temporal Mesial L, and Pons. A statistically significant result indicates in this case that the relationship between the Z-scores and the changing β-value or AC is unlikely to be due to chance or randomness. That is, there was a significant difference in the means of the Z-scores as the β-value or AC changed.

3.2. Z-Score versus β-value

The effects on the Z-Scores when varying the β-value are illustrated in Figure 4. The figure shows data from one patient for all cortical regions. As the β-value increased, the Z-Score decreased. This trend was observed for all cortical regions. In general, the figure also demonstrates how CortexID expresses its Z-Scores. As observed for some regions, for example Prefrontal Medial R and Prefrontal Medial L, the Z-Score reached a significant level, that is -2 or below. This could indicate a pathological result for this patient specifically, while other cortical regions remained within the acceptable healthy Z-Score range. Figure 5 illustrates the difference in absolute Z-Scores from one patient and one cortical region when using ATLAS AC compared to ZTE AC with respect to the β-value. In general, ATLAS AC resulted in a lower Z-Score compared to ZTE AC. Both AC methods yielded a gradually decreasing Z-Score with

an increasing β-value.

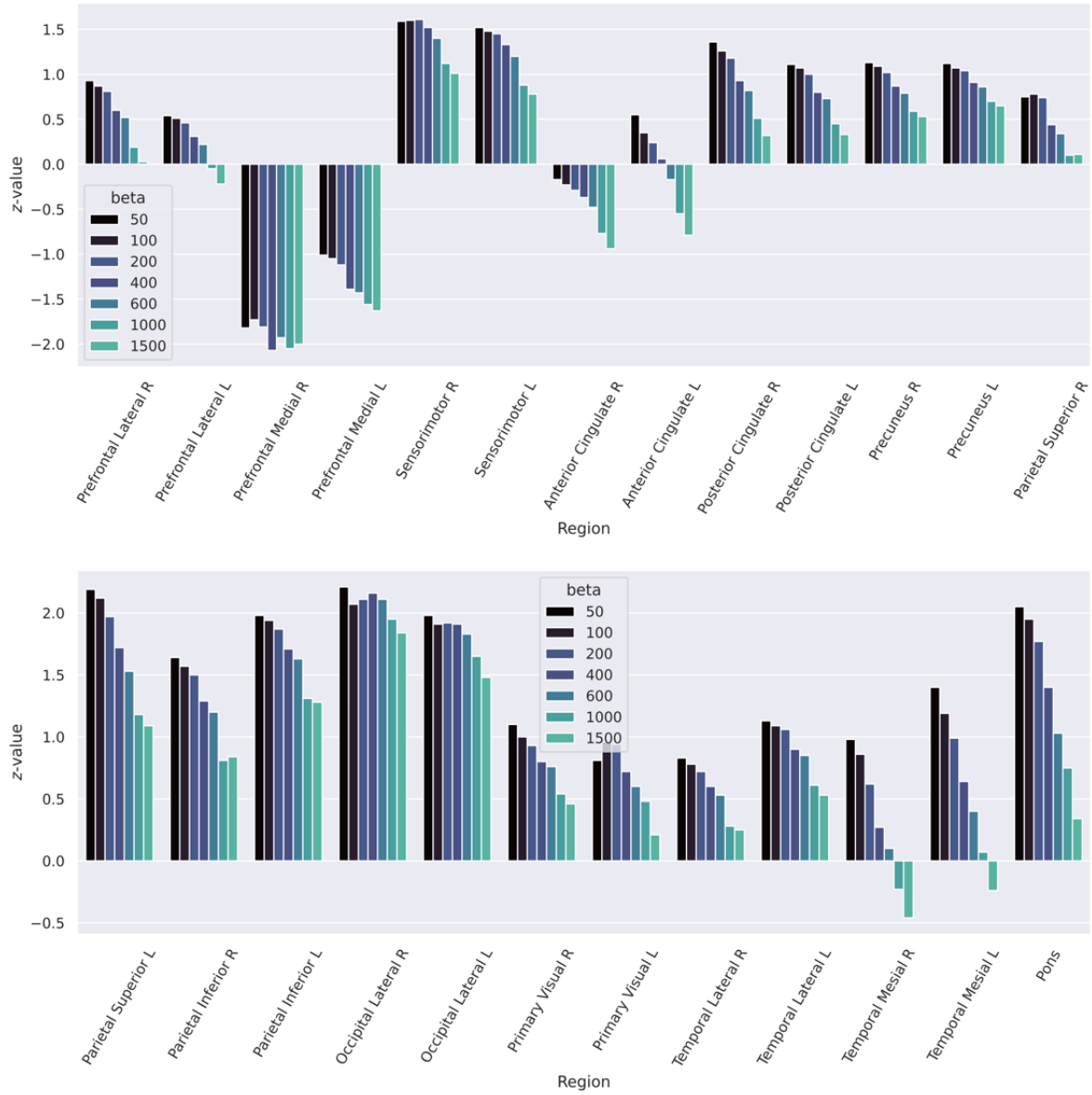

Figure 4: Z-Scores plotted against varying β-values for all cortical regions. Each staple represents a β-value. As the β-value increased, the Z-Score decreased across all cortical regions. The data in this image represents the Z-Scores from one patient.

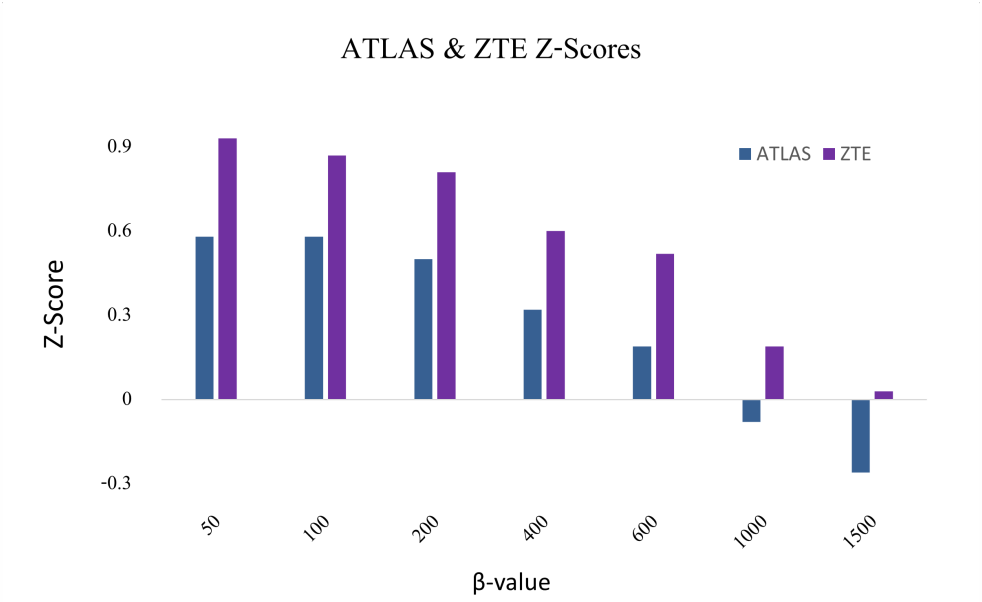

Figure 5: Z-Score difference when utilizing ATLAS AC versus ZTE AC. A higher Z-Score is obtained when using ZTE AC. Z-Scores from both ATLAS AC and ZTE AC decreased as the β-value increased.

3.3. Visual representation

A visual representation of the varying impact of image parameters on image quality is displayed in Figure 6. The figure depicts how ATLAS AC, ZTE AC, and varying β-values affect a brain PET image from one patient with the BPL reconstruction algorithm. A lower β-value resulted in sharper and noisier images, while a higher β-value resulted in blurrier images but with less noise. Visually, the impact of ATLAS AC compared to ZTE AC on the image quality did not differ significantly. Red and orange areas in the image represent higher intensities, while blue and green areas represent lower intensities. Figure 7 takes a closer look at images from Figure 6, showcasing how the choice of AC and the β-value affects the image quality. The image compares clinically used β-values, typically ranging between a β-value of 200 and 600. Once again, the lower β-value resulted in sharper image quality. Upon closer inspection, ATLAS AC showed a minuscule amount of preserved sharpness compared to ZTE AC, though the difference is almost unnoticeable.

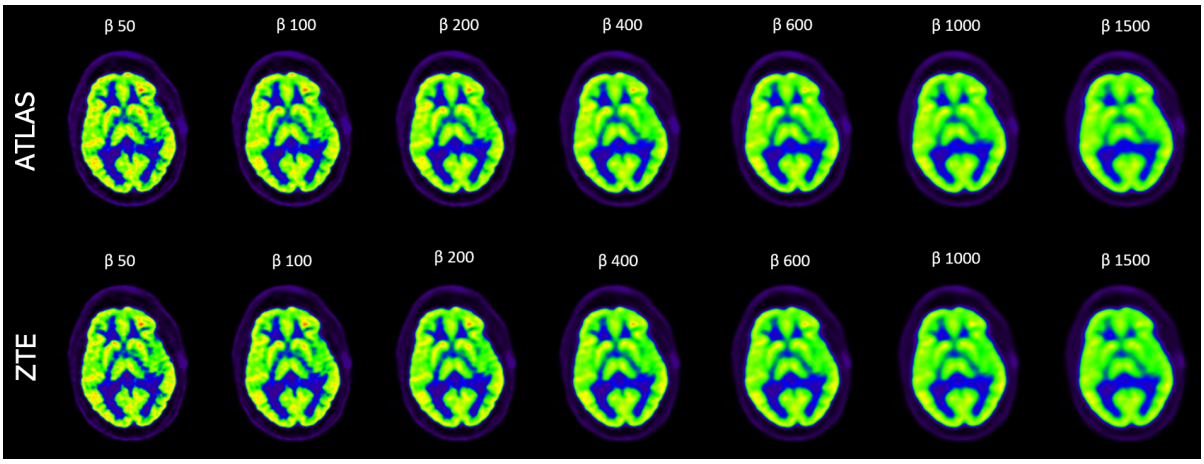

Figure 6: A visual illustration of how the ATLAS AC, ZTE AC and β-value affects the image quality in brain PET. The images are all taken from the same patient, where the upper row images were reconstructed with ATLAS AC and the lower row with ZTE AC. The seven β-values for each AC are displayed. A lower β-value resulted in sharper and noisier images, while a higher β-value resulted in blurry and less noisy images.

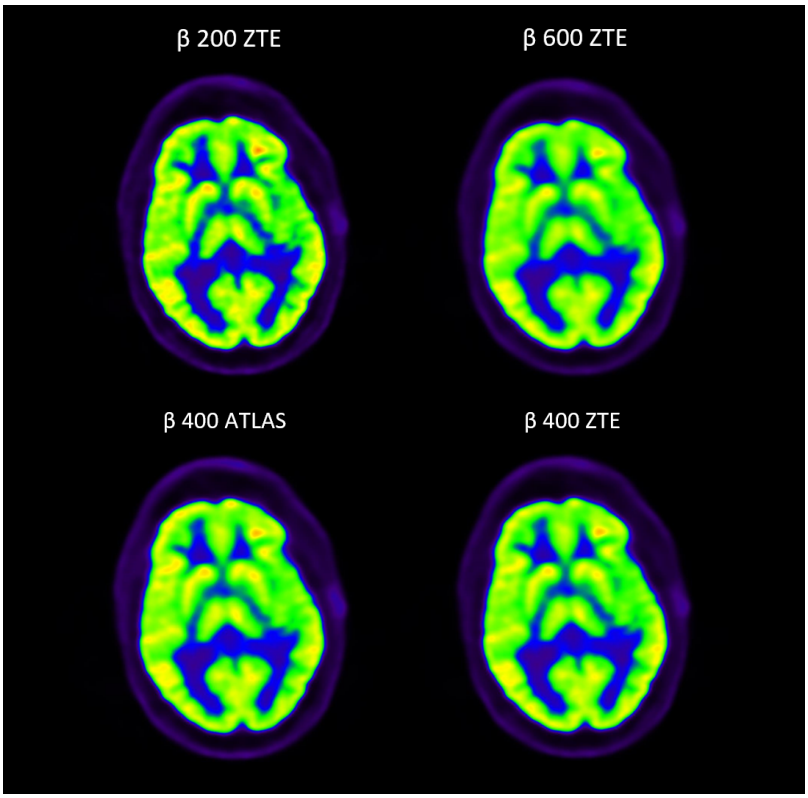

Figure 7: A closer inspection on images from figure 6. The upper two images depicts the image quality of β200 and β600 both with the same ZTE AC. The two lower images represents how the choice of AC affects the image quality, where the β-value remained constant.

3.4. Image quantification

A VOI was applied on all 14 brain PET images from one patient, as shown previously in figure 6, where the max-, mean- and peak-SUV were extracted and plotted against the varying β-value. Two types of VOI's were applied: one on a uniform, homogeneous background (figure 9) and one on an high radioactive tracer uptake region compared to the background (figure 8). This was done in order to evaluate how

the SUV's changed with respect to the varying β-value and the radioactive tracer uptake in comparison to the background. Figure 8 demonstrates the max-, mean- and peak-SUV on a high tracer-uptake region with a low tracer-uptake in the background in comparison, for ATLAS AC and ZTE AC respectively. All of the max-, mean- and peak-SUV decreased as the β-value increased. In general, ZTE AC entailed a higher SUV value compared to ATLAS AC. The max-SUV decreases faster than the mean- and peak-SUV initially. In figure 9, the mean-SUV is relatively unaffected by the β-value compared to the mean-SUV in figure 8.

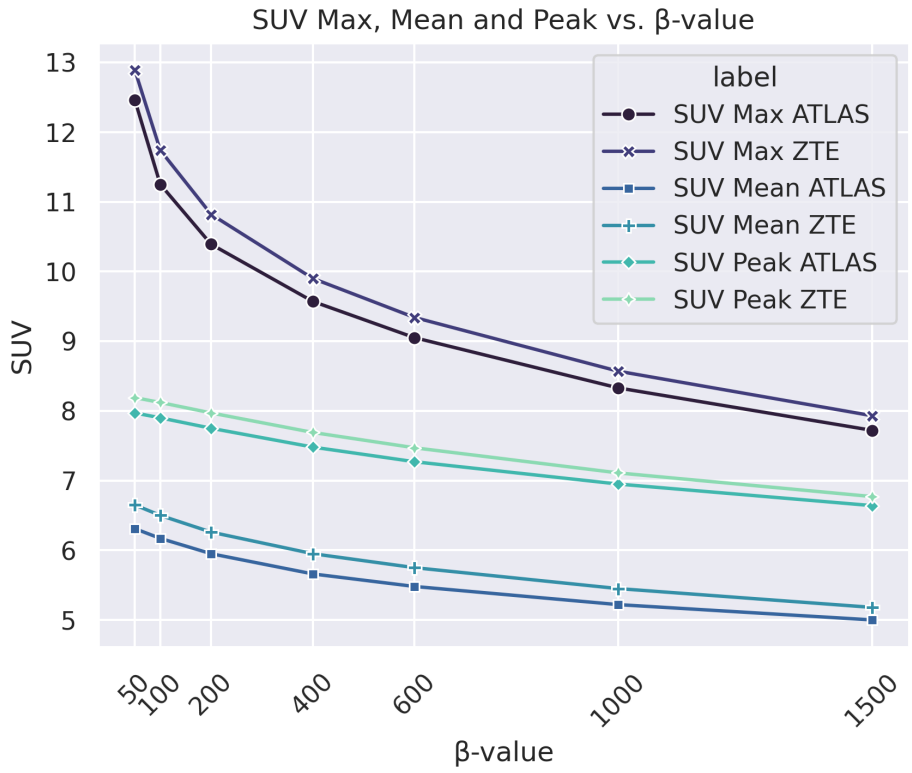

Figure 8: SUV's from a VOI on a high radioactive tracer uptake region compared to the background. The max-, mean- and peak-SUV are plotted against the varying β-value. All SUV's decrease as the β-value increases. The max-SUV decreases at a faster rate than the mean- and peak-SUV initially. The SUV's are plotted for ATLAS AC and ZTE AC respectively.

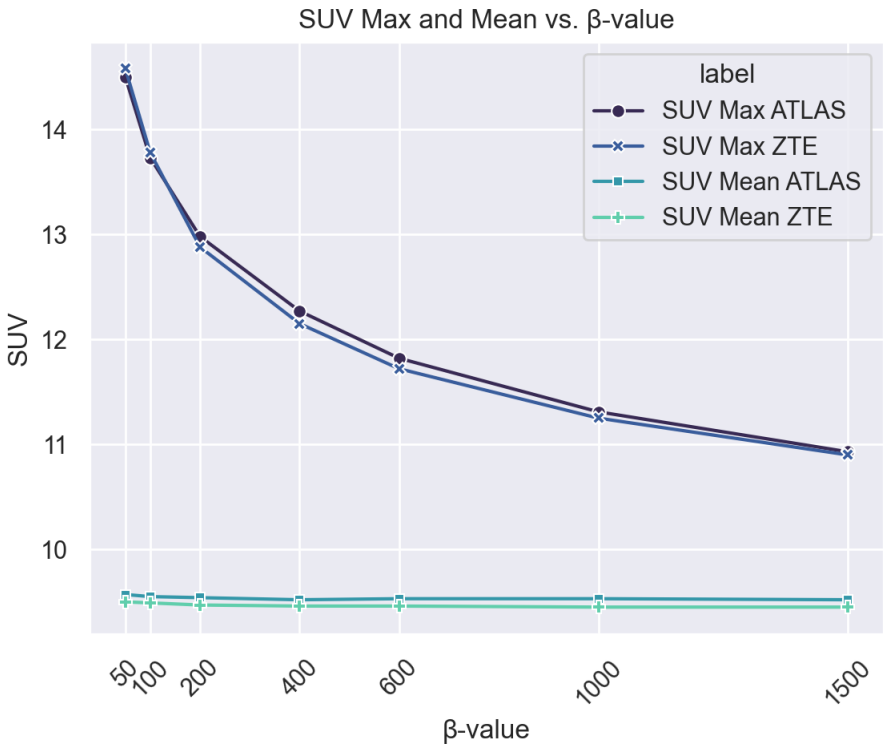

Figure 9: SUV's from a VOI on an uniform, homogeneous background. The max- and mean-SUV are plotted against the varying β-value. Both SUV's decreases as the β-value increases. The max-SUV decreases at a faster rate than the mean-SUV initially. The SUV's are plotted for ATLAS AC and ZTE AC respectively.

3.5. CortexID normal database

An averaging of the four healthy patients' Z-Scores across the varying β-value and all cortical regions for ATLAS AC and ZTE AC respectively was computed. Additionally, OSEM reconstruction with three iterations, 16 subsets with a 5 mm Gaussian filter was added as a category with $\beta = 0$, illustrated in Figure 10. The OSEM reconstruction parameters reflected the normal database performance the most. Consistent with previous observations, the Z-Score decreased as the β-value increased. This comparison aimed to assess how the normal database reconstruction parameters compare with the BPL reconstructions employed in our study. Since only healthy patients were included in this plot, it was hypothesized that the Z-Score would approach zero as the β-value decreased, given that the normal database was absent of any β-values. A reconstruction with the OSEM parameters resulted in a slight drop in the Z-Score compared to those from BPL reconstruction with a low β-value.

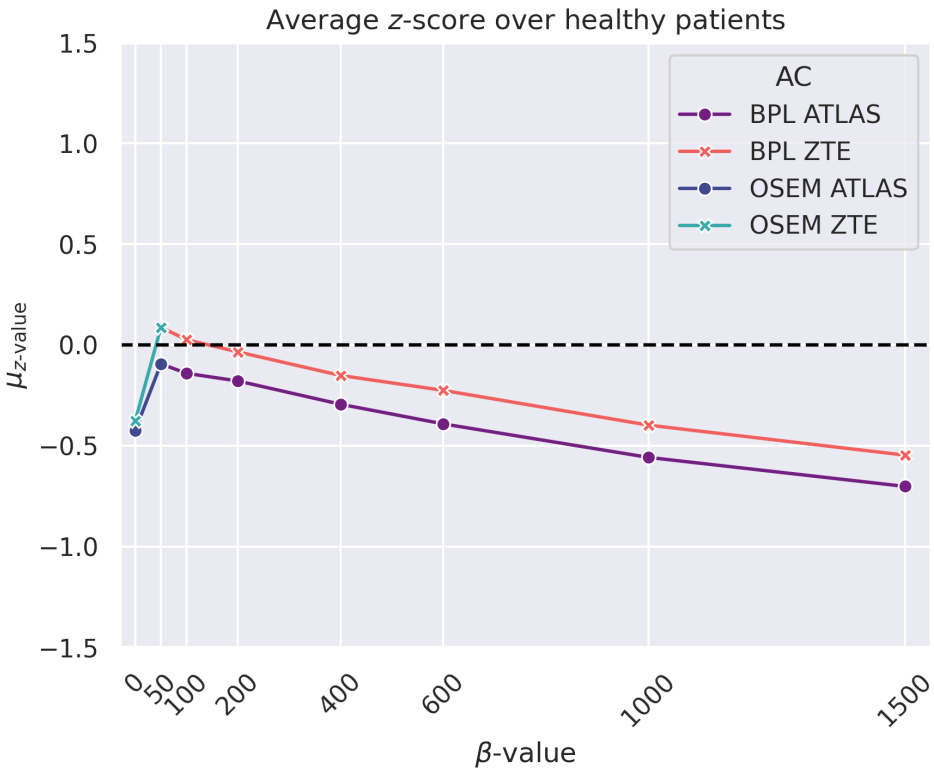

Figure 10: An illustration of an averaging of the four healthy patients' Z-Scores across the varying β-value and all cortical regions. The OSEM reconstruction parameters were three iterations, 16 subsets and with a 5 mm Gaussian filter. The black horizontal line is located at y=0. As the β-value increases the Z-Score decreases. The OSEM reconstruction located at β=0 resulted in a slight drop of the Z-Score compared to the BPL reconstructions with a low β-value. The averaging was computed for ATLAS AC and ZTE AC respectively.

4. Discussion

CortexID software is an effective tool for quantification and interpretation of brain PET images, allowing visualizations of functional information while also including anatomical information from an MR or CT image. It is however important to understand how the software works and operates, and which factors and parameters that needs to be considered prior to its utilization. From a statistical point of view, the choice of the β-value in the BPL reconstruction algorithm affected the Z-Score. The RMA analysis confirmed there was a statistical significance ($P<0.05$) for all cortical regions except for Parietal Superior R using ATLAS AC. This implies that it is important to consider which β-value is to be applied for image reconstruction when utilizing CortexID. Furthermore, the choice of the AC also showed statistical significant results ($P<0.05$) for all cortical regions except for Temporal Mesial R, Temporal Mesial L and Pons. This means, from a statistical point of view, that the Z-Score will differ depending on the chosen AC. In this study, we have simply compared ATLAS AC and ZTE AC, where neither is deemed superior nor chosen as a reference AC method. Instead, our emphasis lies in comparing their performances, with the understanding that the choice of AC method should ideally have no significant impact on the Z-scores. In addition, our study have used data from PET/MR examinations and not from PET/CT examinations as used in the CortexID normal database. Because of this, it is unknown which AC is the reference or ideal to employ within CortexID. It is also unknown precisely which reconstruction parameters were used to construct the CortexID normal database.

It is crucial to emphasize that statistical significance does not always align with clinical relevance. What may be regarded as statistical significant mathematically may not necessarily carry the same weight in a clinical context. This is evident in figure 4, where the Z-Score decreases more rapidly with increasing β-values in Temporal Mesial R and Temporal Mesial L compared to other cortical regions. While this confirms the statistical significance, it also indicates that the Z-Score's rate of change varies across cortical regions. Additionally, in some cases the Z-Score can transition into a pathological result ($Z < -2.0$), as seen in Prefrontal Medial L in Figure 4, leading to false-positive outcomes. If the chosen β-value was within a clinically relevant range (β150-β400), a patient might be deemed healthy unless an extreme β-value, like 1500, is considered. The difference in the Z-Score's rate of change across cortical regions and possible transitions into pathological results may impact the clinical image interpretation. Regarding the choice of the AC, the statistical analysis indicates a substantial difference between ATLAS AC and ZTE AC, with ZTE AC consistently yielding higher Z-Scores compared to ATLAS AC. However, from a clinical perspective, the choice of the AC appears less influential, as the averaged the Z-Scores from all the patients did not show a significant difference. As mentioned earlier, neither ATLAS AC or ZTE AC is considered to be a reference AC or superior to the other, as it can only be concluded that there is a statistical significance between them in mathematical contexts and of lesser importance in clinical contexts regarding which AC is to be employed.

As seen in Figure 6 and 7, a lower β-value results in sharper but noisier images and a higher β-value results in blurrier but less noisier images. This result aligns consistently with the β-value's effect on the image quality, that is a trade-off between image sharpness and noise levels [25–27]. The impact of the AC on image appearance did not differ significantly between ATLAS AC and ZTE AC to the naked eye. The ZTE AC results in ever so slight blurrier images compared to ATLAS AC, though this is negligible as it is almost unnoticeable to the eye.

According to the results from Figure 6, the optimal β-value should lie within β100-β200 in terms of image quality to the naked eye. However, it is important to emphasize that only one physician analyzed the images from Figure 6, and images from only one patient were used. That is, there were no proper evaluation of image noise levels and sharpness, the conclusion in this context is purely based on the obtained results from Figure 6 and what could be detected to the naked eye. Further research and analysis is needed to assess the relationship between image quality and varying β-values when using BPL reconstruction. The results from Figure 6 are not enough to confidently conclude which β-value is optimal for a physician. Nonetheless, a previous study investigated the impact of the β-value on readers ability to detect brain metastasis in PET/CT images [28]. The study is consistent with the optimal choice of the β-value in PET/MR images from our study. They found that a β-value between 100 and 200 enabled the readers to detect the brain metastasis, while metastasis being faintly present with a β-value of 300. It remains arguable whether β300 is appropriate to use and it is somewhat subjective, though it is certain that higher β-values between 600-700 are unsuitable for brain metastasis detection in PET/CT images. Though it is important to highlight that the present study has only focused on PET/MR images and the analysis of neurodegenerative diseases and not oncology cases or PET/CT images.

As the β-value increased, the max-, mean- and peak-SUV decreased, measured from a VOI in an area with high radioactive tracer uptake relative to it's background, which is illustrated in Figure 8. The max-SUV decreased and the mean-SUV was unaffected as the β-value increased, measured from a VOI in an

area with a homogeneous radioactive tracer uptake, showcased in figure 9. A previous study evaluated how the β-value affects the PET image quality and quantification for small pulmonary nodules [25]. The max-, mean- and peak-SUV parameters were investigated with the utilization of partial volume effect correction (PVC). Before any PVC was applied, all of the SUV's decreased as the β-value increased for their lesion-size groups, which aligns with the results in Figure 8 in the present study.

The study also emphasizes the importance of considering the partial volume effect (PVE) which is when the radioactive tracer uptake is underestimated in lesions smaller than two times of the systems spatial resolution. The PVE consists of so-called "spill-in" and "spill-out" effects. Spill-in effects occur when activity from hot regions infiltrate, or spill-in, into nearby lesions with a lower activity. This results in an overestimation of the SUV's in those regions. On the other hand, when considering SUV's on lesions with high radioactive tracer uptake, the activity is usually underestimated due to the loss, or spill-out, of activity to neighboring regions with a lower activity [25]. In the case of a heterogeneous area, that is, an area where boundaries or structures between different tissues are present, the PVE is more likely to be a problem than in a homogeneous area. This may explain why the mean-SUV in figure 8 decreases in the present study while remaining unchanged in figure 9 as the β-value increases.

The max-SUV decreases as the β-value increases possibly since the max-SUV is the highest level of radioactive tracer uptake in a ROI, which tend to be affected by the noise levels in a PET image. An increasing β-value lowers the noise level, hence the declination of max-SUV. The mean-SUV is the averaged radioactive tracer uptake in a ROI, and as mentioned before, it is primarily affected by the PVE. In a heterogeneous area, the β-value will have a definite impact on the mean-SUV. The peak-SUV is the average SUV in a volume (specifically 1 mL) that includes the highest value of the mean. In most of the cases the peak-SUV does not include the pixel with the max-SUV, making it less likely to be dependent on noise levels and lesion delineations. However, if a high β-value is used, then the image could be smoothed out significantly which may lead to a broader and lower peak intensity in the ROI, which decreases the peak-SUV.

An additional reconstruction was conducted for the healthy subjects in the present study using the OSEM reconstruction algorithm with three iterations, 16 subsets and a 5 mm Gaussian filter. This reconstruction reflected the parameters used in CortexID normal database the most upon prior research findings. The purpose of this comparison with the normal database was to evaluate the suitability of BPL reconstruction when utilizing CortexID for clinical diagnostics in PET imaging. Given that the subjects were deemed healthy, it was anticipated that the Z-Score would be close to zero when compared to the normal database reconstruction parameters. The same rationale was applied to the BPL reconstruction with a low β-value, considering that the normal database did not include any β-value due to the absence of a BPL reconstruction. The results illustrated in Figure 10 reveals that as the β-value decreases, the Z-Score seems to converge toward zero. However, when a reconstruction with OSEM was added as β=0, the Z-Score dropped, though still close to zero. It is also observed in the figure that β100-200 for BPL ZTE AC gave a Z-Score close to zero. Based on the results from Figure 10, the optimal β-value should lie within β100-200 when utilizing BPL reconstruction with CortexID. This result is supported by the results from Figure 6, where the optimal beta value lied within β100-200. The results from Figure 10 are more reliable than the results in Figure 6 because of the larger sample size.

However, no definite conclusions can be drawn from Figure 10. This is due to the many limitations

that affects the reliability of the results. The biggest limitation is the lack of healthy patients included in the plot. Due to the lack of time, only four patients were included, whereupon two of them were deemed as healthy by health professional despite the fact that they still had slight radioactive tracer uptake deviations. In addition, an averaging was performed of all the patients including the Z-Scores from each cortical region. This could indicate unreliable results because each cortical region responds differently to radioactive tracer uptake across all the healthy patients, and each cortical region needs to be regarded as its own parameter.

Moreover, it remains unclear whether OSEM reconstruction with three iterations, 16 subsets and a 5 mm Gaussian filter truly reflects the normal database performance. These parameters were selected purely based on prior research findings. In reality, the normal database parameters utilized by GE Healthcare were different than the parameters used in the present study, because the PET/MR console used did not have the options for an identical normal database reconstruction. Despite the limitations, it remains worthwhile to examine how the Z-Score is affected when using other reconstruction parameters compared to the normal database. This can be accomplished with an adequate amount of healthy patients, while also regarding each cortical region as its own parameter and confirming that the OSEM reconstruction parameters reflect the normal database.

Out of the sick patients included in the study, two of them had significantly deviated Z-Scores compared to the rest of the patients. It was suspected that CortexID may had incorrectly co-registered the patient MR image. After the OSEM reconstruction parameters were applied on these two deviated sick patients, the Z-Score remained relatively unchanged which indicates that it is not an error of a reconstruction algorithm in itself. However, upon closer inspection of both patient's images in CortexID, it was noted that both had no error in image registration, rather, it was a case of medical condition deviations. One of the patients had a significantly decrease in frontal lobe, and of a lesser degree in their temporal lobe, which strongly indicates a typical outcome of frontotemporal dementia (FTD). The other patient had a significant radioactive tracer uptake decrease in their cerebellum, which indicates that using cerebellum whole as a reference region is deemed improper. This patient also had a decrease in their brain stem and pons, which is a typical case of atypical Parkinson's syndrome.

In general, one limitation of the present study is the inclusion of a limited number of subjects. Only 25 subjects were included, with only four being healthy. To enhance the reliability of the results, a larger number of subjects should be involved, especially those with identical neurodegenerative diseases and staging within that disease. This is important because the study encompassed patients with a diverse range of neurodegenerative diseases at different stages. Some patients had advanced Alzheimer's disease, while others showed only early signs. Another potential source of error in this study is the size of the applied VOIs on the PET images. When considering the impact of PVE on SUVs, a uniform VOI should be applied to the region of interest or lesion to avoid including delineations. In this study, the applied VOI on the high radioactive tracer uptake region was not perfectly uniform, although the effect of the β-value on the SUVs still aligned with previous research findings.

It would be insightful to investigate how CortexID performs compared to *syngo*.via, by comparing image quality and quantification from both software's. This could reveal potential superior aspects in utilizing CortexID instead of *syngo*.via. Another parameter worth examining is if the imaging modality, such as PET/MR compared to PET/CT, could alter CortexID Z-Score results. In addition, it is also advantageous

to evaluate if the chosen MRI sequence could yield different Z-Scores, since the present study has only used AX T2 PROPELLER sequence. Other parameters such as pixel size, FOV, with and without TOF, with and without PSF, iterations and subsets, and filter size are also beneficial to assess regarding how they affect the Z-Score. Lastly, but of equal importance, it is valuable to investigate whether CortexID effectively and correctly facilitates patient diagnosis. This can be achieved by comparing the Z-Scores and images with those generated using normal database parameters and with *syngo*.via.

5. Conclusion

In conclusion, our study demonstrates that the choice of the β-value significantly impacts the image Z-score outcomes in CortexID for brain PET/MR imaging and should thus be carefully considered in clinical applications. Additionally, ZTE AC yields higher Z-Scores compared to ATLAS AC, with negligible differences in image comparison. Furthermore, variations in β-values impact SUV quantification, which is crucial for accurately assessing tracer uptake in cortical brain regions. The present study suggests an optimal β-value between 100-200 for CortexID quantification of uptake in brain regions. However, due to limitations and a small sample size, further research is required to confirm the ideal β-value.

Acknowledgement

I would like to express my sincere gratitude to Esmaeil Mehrara, Martijn van Essen, Jesus Lopez Urdaneta and Susanna Jakobson for their expert guidance, wise counsel and dedicated support. A special appreciation goes to Esmaeil Mehrara for his patience, insightful tips and tutelage, which have been crucial to the success of the project. I am also grateful to my family and friends for their encouragement and motivational endeavors.

References

1. Van Schependom, J., & Dhaeseleer, M. (2023). Advances in neurodegenerative diseases. *Journal of clinical medicine*, *12*(5), 1709.
2. Morigi, J., Kovaleva, N., & Phan, S. (2022). Spotlight on:dynamic pet/ct imaging. *Clinical and Translational Imaging*, *10*(3), 239–241.
3. Khan, S. (2014). Creating positron emission tomography facility in remote areas. *Indian Journal of Nuclear Medicine: IJNM*, *29*(4), 208.
4. Pichler, B. J., Judenhofer, M. S., & Pfannenberg, C. (2008). Multimodal imaging approaches: Pet/ct and pet/mri. *Molecular Imaging I*, 109–132.
5. Lindström, E., Oddstig, J., Danfors, T., Jögi, J., Hansson, O., & Lubberink, M. (2020). Image reconstruction methods affect software-aided assessment of pathologies of [18f] flutemetamol and [18f] fdg brain-pet examinations in patients with neurodegenerative diseases. *NeuroImage: Clinical*, *28*, 102386.
6. Rogasch, J. M., Hofheinz, F., van Heek, L., Voltin, C.-A., Boellaard, R., & Kobe, C. (2022). Influences on pet quantification and interpretation. *Diagnostics*, *12*(2), 451.
7. General Electric Healthcare. (2015). *Cortexid suite*. General Electric Company.
8. Javed, K., Reddy, V., & Lui, F. (2019). Neuroanatomy, cerebral cortex.
9. Jawabri, K. H., & Sharma, S. (2019). Physiology, cerebral cortex functions.
10. Sandilyan, M. B., & Dening, T. (2019). What is dementia. *Evidence-based practice in dementia for nurses and nursing students*.
11. Jellinger, K. A. (2018). Dementia with lewy bodies and parkinsons disease-dementia: Current concepts and controversies. *Journal of neural transmission*, *125*, 615–650.
12. Riedl, L., Mackenzie, I. R., Förstl, H., Kurz, A., & Diehl-Schmid, J. (2014). Frontotemporal lobar degeneration: Current perspectives. *Neuropsychiatric disease and treatment*, 297–310.
13. Hoh, C. K. (2007). Clinical use of fdg pet. *Nuclear medicine and biology*, *34*(7), 737–742.
14. Marcus, C., Mena, E., & Subramaniam, R. M. (2014). Brain pet in the diagnosis of alzheimers disease. *Clinical nuclear medicine*, *39*(10), e413.
15. Townsend, D., et al. (2004). Physical principles and technology of clinical pet imaging. *Annals-Academy of Medicine Singapore*, *33*(2), 133–145.
16. Jiang, W., Chalich, Y., & Deen, M. J. (2019). Sensors for positron emission tomography applications. *Sensors*, *19*(22), 5019.
17. Fahey, F. H. (2002). Data acquisition in pet imaging. *Journal of nuclear medicine technology*, *30*(2), 39–49.

18. Markiewicz, P., Thielemans, K., Schott, J., Atkinson, D., Arridge, S., Hutton, B., & Ourselin, S. (2016). Rapid processing of pet list-mode data for efficient uncertainty estimation and data analysis. *Physics in Medicine & Biology*, *61*(13), N322.

19. Lucignani, G., Paganelli, G., & Bombardieri, E. (2004). The use of standardized uptake values for assessing fdg uptake with pet in oncology: A clinical perspective. *Nuclear medicine communications*, *25*(7), 651–656.

20. Wagenknecht, G., Kaiser, H.-J., Mottaghy, F. M., & Herzog, H. (2013). Mri for attenuation correction in pet: Methods and challenges. *Magnetic resonance materials in physics, biology and medicine*, *26*, 99–113.

21. Sekine, T., Buck, A., Delso, G., Ter Voert, E. E., Huellner, M., Veit-Haibach, P., & Warnock, G. (2016). Evaluation of atlas-based attenuation correction for integrated pet/mr in human brain: Application of a head atlas and comparison to true ct-based attenuation correction. *Journal of Nuclear Medicine*, *57*(2), 215–220.

22. Wiesinger, F., Sacolick, L. I., Menini, A., Kaushik, S. S., Ahn, S., Veit-Haibach, P., Delso, G., & Shanbhag, D. D. (2016). Zero te mr bone imaging in the head. *Magnetic resonance in medicine*, *75*(1), 107–114.

23. Sousa, J. M. (2021). *Assessment of attenuation correction methods for quantitative neuro-pet/mr* [Doctoral dissertation, Acta Universitatis Upsaliensis].

24. De Pierro, A. R., & Yamagishi, M. B. (2001). Fast em-like methods for maximum" a posteriori" estimates in emission tomography. *IEEE transactions on medical imaging*, *20*(4), 280–288.

25. Wu, Z., Guo, B., Huang, B., Zhao, B., Qin, Z., Hao, X., Liang, M., Xie, J., & Li, S. (2021). Does the beta regularization parameter of bayesian penalized likelihood reconstruction always affect the quantification accuracy and image quality of positron emission tomography computed tomography? *Journal of Applied Clinical Medical Physics*, *22*(3), 224–233.

26. Tatsumi, M., Soeda, F., Kamiya, T., Ueda, J., Katayama, D., Matsunaga, K., Watabe, T., Kato, H., & Tomiyama, N. (2021). Effects of new bayesian penalized likelihood reconstruction algorithm on visualization and quantification of upper abdominal malignant tumors in clinical fdg pet/ct examinations. *Frontiers in Oncology*, *11*, 707023.

27. Te Riet, J., Rijnsdorp, S., Roef, M. J., & Arends, A. J. (2019). Evaluation of a bayesian penalized likelihood reconstruction algorithm for low-count clinical 18 f-fdg pet/ct. *EJNMMI physics*, *6*, 1–14.

28. Liberini, V., Pizzuto, D. A., Messerli, M., Orita, E., Grünig, H., Maurer, A., Mader, C., Husmann, L., Deandreis, D., Kotasidis, F., et al. (2022). Bsrem for brain metastasis detection with 18f-fdg-pet/ct in lung cancer patients. *Journal of Digital Imaging*, *35*(3), 581–593.

Appendix

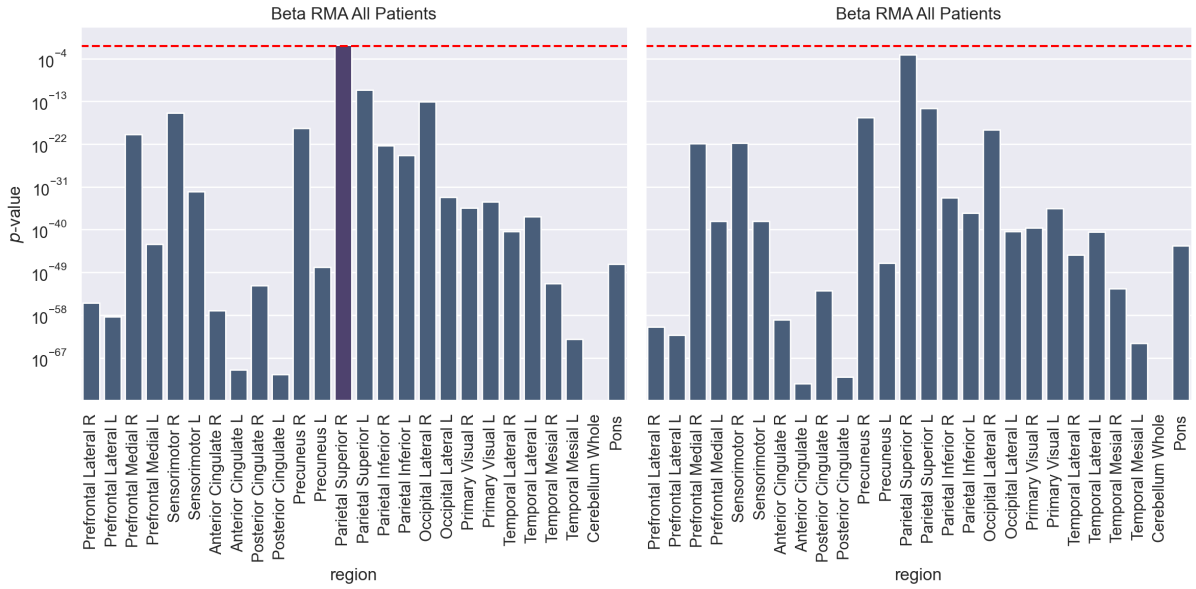

Figure 11: Results of the Repeated Measures ANOVA (RMA). The data obtained from ATLAS AC is depicted in the right plot, while the left plot illustrates the data from ZTE AC. The y-axis shows the p-value for each cortical region on the x-axis. The red dashed horizontal line is located on y = 0.05, which indicates that all values below that line is considered statistically significant. Parietal Superior R (P>0.05) with ATLAS AC was statistically insignificant.

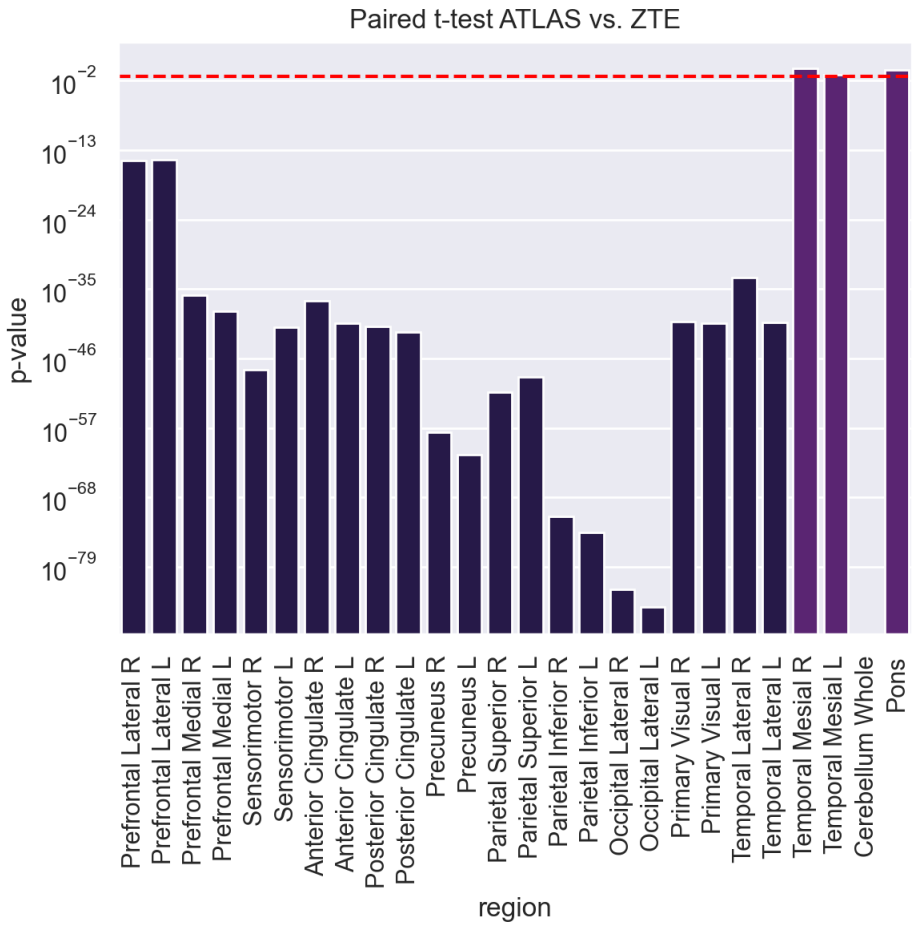

Figure 12: Results of the paired t-test where means of the Z-Scores from ATLAS AC and ZTE AC were compared. The red dashed horizontal line is located on y = 0.05, which indicates that all values below that line is considered statistically significant. Temporal Mesial R, Temporal Mesial L and Pons were statistically insignificant (P>0.05).

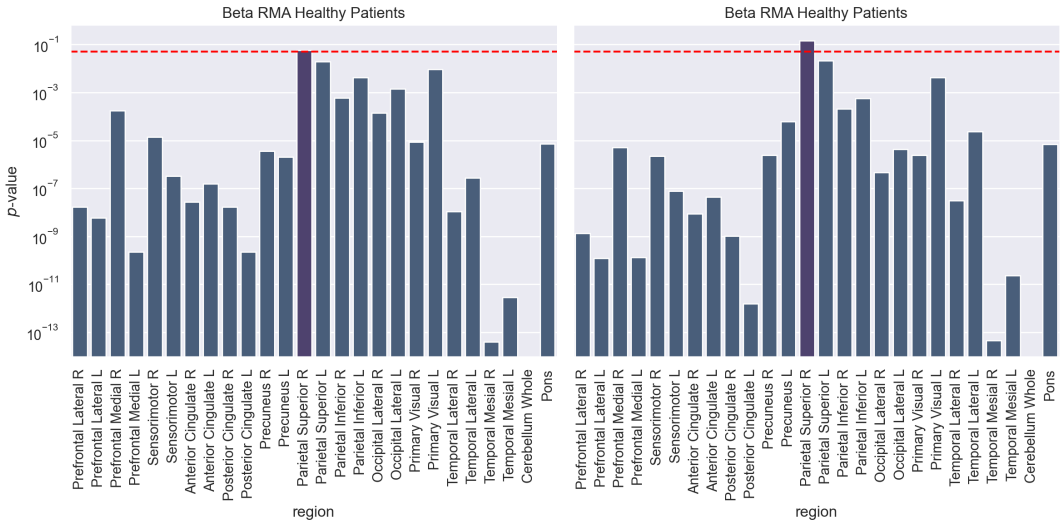

Figure 13: Results of the Repeated Measures ANOVA (RMA) on the healthy patients. The data obtained from ATLAS AC is depicted in the right plot, while the left plot illustrates the data from ZTE AC. The y-axis shows the p-value for each cortical region on the x-axis. The red dashed horizontal line is located on y = 0.05, which indicates that all values below that line is considered statistically significant. Parietal Superior R (P>0.05) with on both AC were statistically insignificant.

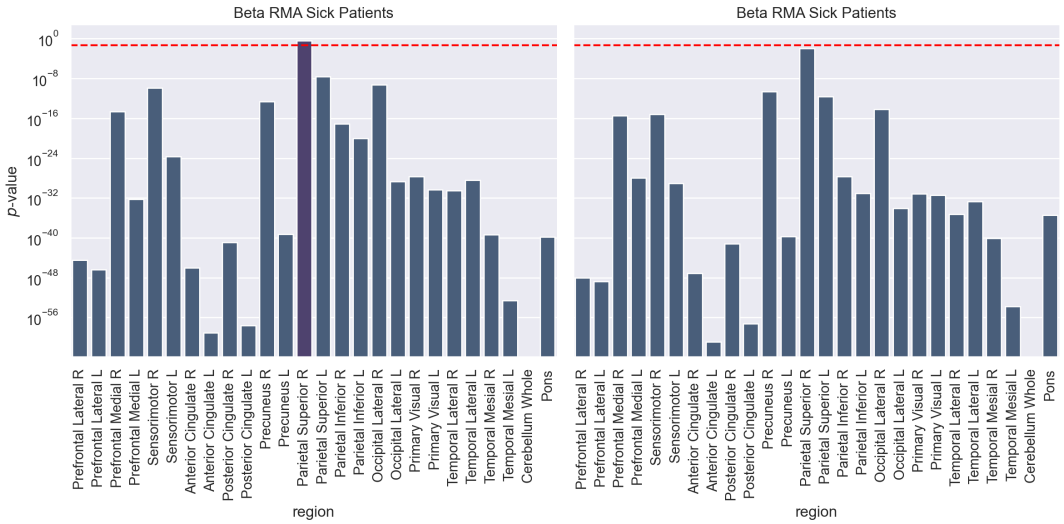

Figure 14: Results of the Repeated Measures ANOVA (RMA) on the sick patients. The data obtained from ATLAS AC is depicted in the right plot, while the left plot illustrates the data from ZTE AC. The y-axis shows the p-value for each cortical region on the x-axis. The red dashed horizontal line is located on y = 0.05, which indicates that all values below that line is considered statistically significant. Parietal Superior R (P>0.05) with ATLAS AC was statistically insignificant.

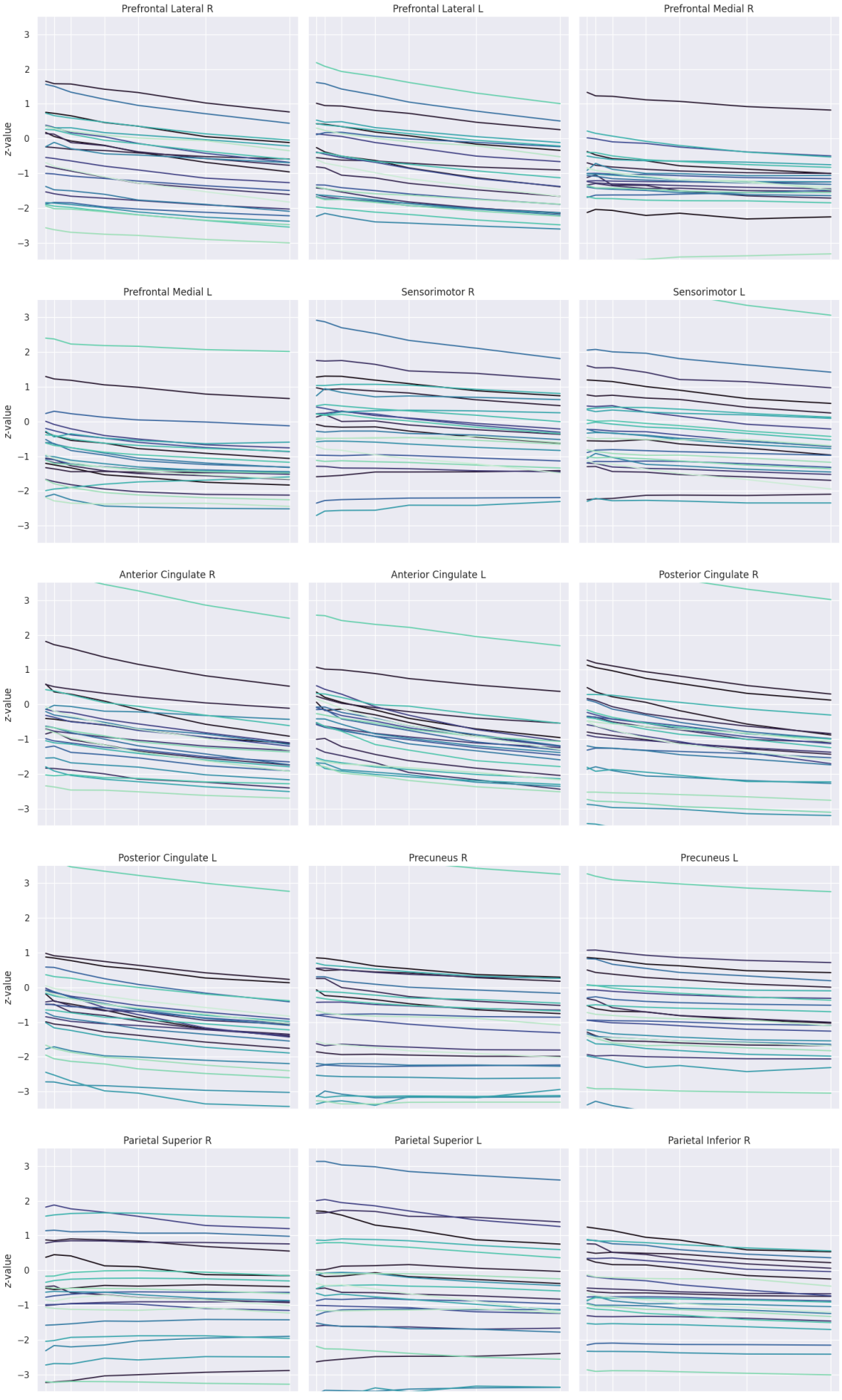

Figure 15: An illustration on how the Z-Score varies with the β-value for all cortical regions.

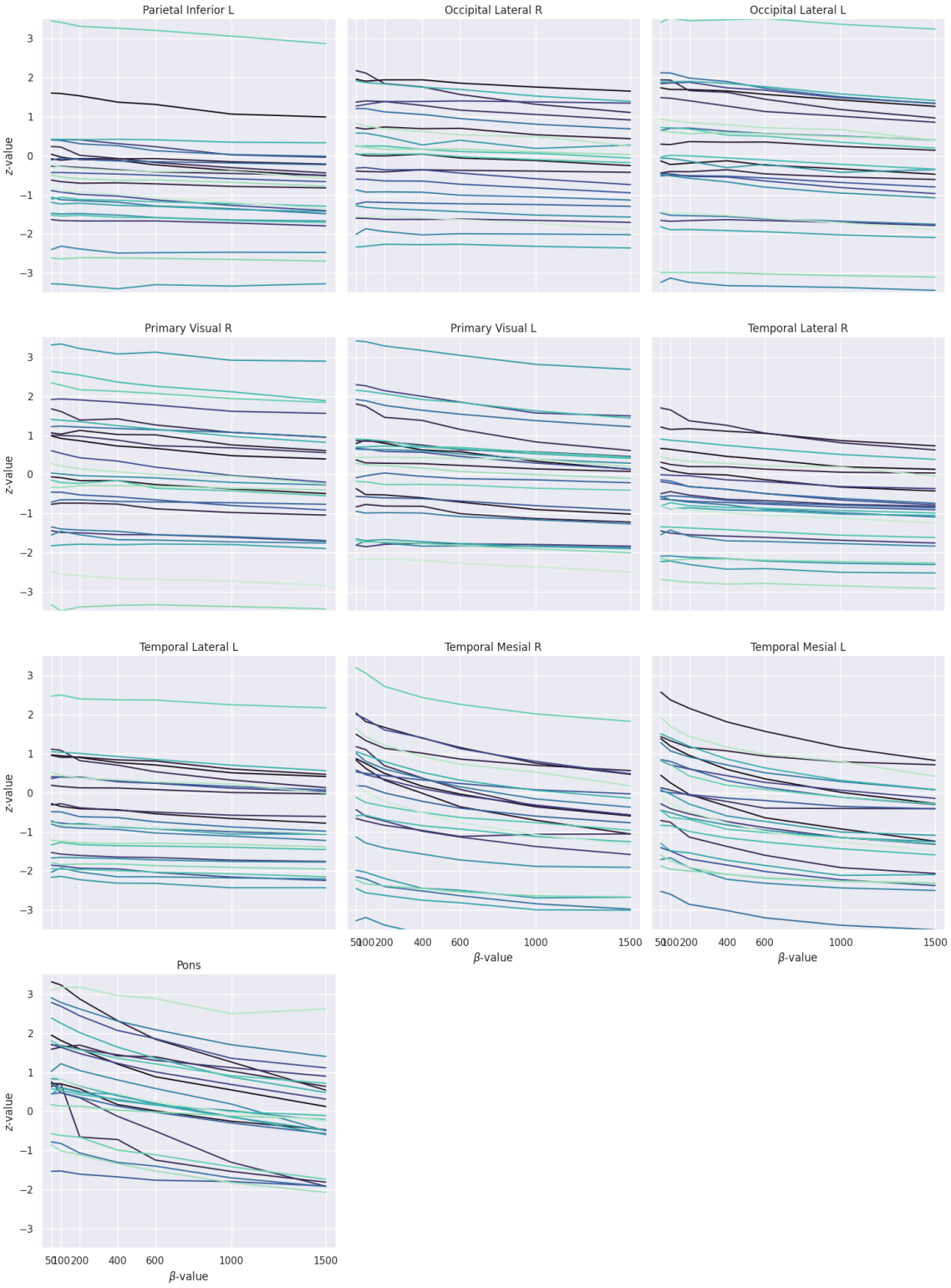

Figure 16: An illustration on how the Z-Score varies with the β-value for all cortical regions.

UNIVERSITY OF
GOTHENBURG